Ion transport in two-dimensional flexible nanoporous membranes

Yechan Noh and Narayana R. Aluru[*]

Department of Mechanical Science and Engineering, University of Illinois at Urbana-Champaign, Urbana, Illinois 61801, United States

* Walker Department of Mechanical Engineering, Oden Institute for Computational Engineering & Sciences, University of Texas at Austin, Austin 78712, United States

[*]*Correspondence: aluru@utexas.edu*

KEYWORDS

Ion transport, metal–organic framework, hexaaminobenzene, graphene nanomesh, vibrational coupling, flexible membrane, 2D membrane, nanopore, hydration shell.

SUMMARY

Ion transport is a fundamental mechanism in living systems that plays a role in cell proliferation, energy conversion, and maintaining homeostasis. This has inspired various nanofluidic applications such as electricity harvesting, molecular sensors, and molecular separation. Two dimensional (2D) nanoporous membranes are particularly promising for these applications due to their ultralow transport barriers. We investigated ion conduction across flexible 2D membranes via extensive molecular dynamics simulations. We found that the microscopic fluctuations of these membranes can significantly increase ion conductance, for example, by 320% in Cu-HAB with 0.5 M KCl. Our analysis of ion dynamics near the flexible membranes revealed that ion hydration is destabilized when the membrane fluctuated within a specific frequency range leading to improved ion conduction. Our results show that the dynamic coupling between the fluctuating membrane and ions can play a crucial role in ion conduction across 2D nanoporous membranes.

INTRODUCTION

Living systems, including humans, rely on ion transport as a fundamental mechanism for various physiological processes, such as maintaining homeostasis[1], regulating cell proliferation[1], generating electricity[2], and producing energy-storage molecules[3,4]. Ion transport across nanometer-sized pores exhibits unique characteristics such as selective ion transport[5–8], activation by stimuli[9,10], and mechanosensitive ion transport[11,12]. These features of ion transport have inspired a wide range of applications such as osmotic power generation[13,14], ion separation[15,16], DNA sequencing[17,18], and water purification[19–22]. Recently, several 2D nanoporous membranes have been successfully fabricated using bottom-up approaches[23–25] and these advances are expected to further advance nanopore applications owing to their ultralow transport barrier, uniform pore size, high pore density, and excellent flexibility. Several studies have focused on ion-transport phenomena across the 2D membranes providing a microscopic understanding on the effect of diameter[26–28], surface charge density[26,29], functional groups[30], mechanical strain[31,32], ion concentration[26], and pore-pore interactions[33–35]. However, there is a lack of understanding of how the exceptional flexibility of 2D nanoporous membranes affects microscopic ion transport.

Over the past few decades, researchers have studied various aspects of ion transport across 2D nanoporous membranes. In 2008, Sint *et al.*[36] studied ion transport through functionalized graphene nanopores using molecular dynamics (MD) simulations. They demonstrated that a graphene nanopore could be an anion or cation-selective membrane depending on the functional groups. In 2013, He *et al.*[30] presented a computational study demonstrating that a graphene nanopore with 0.43 nm diameter and three carboxylate groups exhibited voltage-dependent selectivity (i.e., cation and anion-selective at low and high voltages, respectively). In 2014, Suk and Aluru[27] studied ion transport in sub-5 nm graphene nanopores using MD simulations. They

demonstrated that the density and mobility of ions in a nanopore deviate from their bulk value, and continuum theory with corrected density and mobility can account for MD simulation results. In 2019, Fang *et al.*[31] studied the effect of mechanical strain on ion conduction through a graphene-embedded crown. They observed strain-sensitive ion transport, where ion current increases by an order of magnitude when 2% strain is applied. In 2020, Noh and Aluru[26] demonstrated that 2D nanopores are electrically imperfect, and ion conductance is not entirely governed by surface conductance. In 2022, Jiang *et al.*[37] demonstrated a pressure-induced enhancement of ion conductance in single-layer graphene nanopores, which cannot be explained by the linear electrokinetic theory. Jiang *et al.* further demonstrated that ion conductance increases due to the pressure-driven transport of capacitively accumulated ions near the graphene surface, creating nonlinear electrohydrodynamic coupling. However, many prior MD simulations overlooked nanopore flexibility, assuming nanopores to be rigid. This assumption may not align with experimental studies, potentially leading to inconsistencies between simulated predictions and experimental results. In our current investigation, we aim to bridge this gap by accounting for nanopore flexibility.

Prior research in the fields of molecular biology and nanofluidics have demonstrated the importance of surface fluctuations in various microscopic phenomena. In 1999, Kohen *et al.*[38] studied biological catalysts and observed that the vibrational modes of enzymes are a major factor in their catalytic activity. In 2001, Bernèche and Roux[8] studied the KcsA potassium channel and observed that the fluctuations of the channel structure can considerably affect the free energy profiles and ion selectivity. In 2004, Noskov *et al.*[5] studied the KcsA channel and observed that carbonyl groups exhibit liquid-like fluctuations that are important for ion selectivity. In 2015, Ma *et al.*[39] studied water transport in a double-walled carbon nanotube and observed that the

longitudinal vibration mode of the CNT creates oscillatory friction and enhances diffusion of confined water. In 2018, Marbach *et al.*[40] theoretically showed that the effective diffusion of confined fluids within wiggling surfaces can be increased or decreased depending on the spectrum of surface fluctuations. In 2021, Noh and Aluru[21] demonstrated that water permeation in a 2D flexible membrane is higher (up to 102%) than that in its rigid counterpart and that water permeation is maximized when the membrane frequency matches the vibrational frequency of water molecules. In subsequent work[41], they demonstrated vibrational coupling-induced enhancement of water transport is more significant in small diameter pores (water flow increases up to 500% in a 0.75 nm diameter pore). In 2022, Lyu *et al.*[42] studied chloride conduction in multilayered COF membranes and concluded that membrane flexibility is an important factor for predicting experimentally measured chloride conductivity.

In the present study, we analyze how the flexibility of 2D nanoporous membranes affects ion transport. We study ion transport considering two different types (flexible and rigid) of nanoporous membranes and observe a considerable difference between ion current in the flexible membrane and its rigid counterpart. To understand the mechanisms arising from the membrane flexibility, we analyze the pore expansion, ion dynamics near the membranes, and microscopic fluctuations of the membrane and nearby ions.

RESULTS AND DISCUSSION

The primary focus of this study is to understand how the flexibility of a membrane affects ion conduction. Toward this, we designed MD simulations as shown in **Figure 1a**. The nanoporous membrane was immersed in an electrolyte solution, and the edges of the membrane were constrained while the rest of the membrane fluctuates freely. For comparison, we also considered a rigid membrane, where all membrane atoms were fixed. A constant external electric field was applied along the z-direction of the system to generate an electrophoretic ion current. We considered two single-layer nanoporous membranes (**Figures 1b and c)**: Cu-HAB[25,43] and GNM-3[21]. GNM-3 is a graphene nanomesh[44]. The graphene-based nanopore membrane was actively studied for various applications[20,22,30,36,45,46] and was recently synthesized on a large scale with a consistent pore size[23]. Cu-HAB[25,43] is a metal–organic framework (MOF)-based 2D membrane. MOF-based membranes have shown great potential in numerous applications[15,19,21,25,47–49]. In this study, GNM-3 and Cu-HAB are hydrogenated and assumed to be defect free. **Figures 1d and e** demonstrate fluctuations in nanoporous membranes where the amplitudes of the fluctuations are a few Angstroms, which is comparable to the size of nanopore we consider. **Figures 1f and g** show the current–voltage response for 2D nanoporous membranes. For both membranes, we observe a linear relation between ion current and applied voltage within the tested voltage range. Interestingly, ion conductance (*i.e.,* the slope of the current–voltage curve) in flexible Cu-HAB is approximately twice that of its rigid counterpart, where mechanical deformations and fluctuations are suppressed.

On the other hand, ion conductance in the flexible GNM-3 membrane is marginally higher (9%) than that of its rigid counterpart. As a result, ion conductance in flexible Cu-HAB is slightly higher than in flexible GNM-3, although the pore size of GNM-3 is 25% higher than that of Cu-HAB.

Figures 2a and b show the number of ion species transported across the membranes over time. The transport of potassium and chloride ions increases linearly and is higher in the flexible membranes compared to their respective rigid counterparts**.** Also, it is shown that both cation and anion currents increase and this results in reduced ion selectivity. Specifically, we measured the anion selectivity using the formula: $S^- = \frac{-I^+}{I^- + I^+}$, where I^- represents anion current and I^+ represents cation current. In rigid Cu-HAB, the anion selectivity is $S^- = 0.68$, but the anion selectivity is reduced to $S^- = 0.49$ in flexible Cu-HAB. This is attributed to the slightly enlarged pore diameter in flexible membrane and the vibrational coupling effect. **Figure 2a and b** show a slight electroosmotic flow that is created by anion selectivity due to the positive charge of the nanopores. This hydrodynamic flow can slightly increase the anion transport, while slightly decreasing the cation transport. We note that the fluctuations of the membrane do not create directional water flow, as the system considered in this work is ideally symmetrical.

To better understand the phenomenon, we conducted parametric studies considering different concentrations of ions, types of ions, and temperatures. **Figure 2c** shows that ion conductance is much higher in flexible Cu-HAB than in its rigid counterpart for all the tested concentrations. Similarly, ion conductance in flexible GNM-3 (**Figure 2d**) is higher than in its rigid counterpart for all the tested concentrations. However, the difference in ion conductance between the flexible and rigid membranes is lower for GNM-3 membranes than for Cu-HAB membranes at the same concentration (**Figure 2i**). Notably, ion conductance in 0.5 M KCl is approximately 320% higher in the flexible Cu-HAB membrane and 130% higher in the flexible GNM-3 membrane than in their respective rigid counterparts. We attribute this to the enhanced ion transport through the membrane surface in low concentration, which will be discussed further

later in this paper. For the types of ions considered (*i.e.,* KCl, NaCl and NaBr), we observed that the conductance was considerably higher in the flexible Cu-HAB membrane (**Figure 2e**) and slightly higher in the flexible GNM-3 membrane (see **Figure 2f**) compared to their rigid counterparts. **Figures 2g and h** show that ion conductance increases with the increase in temperature for both membranes, but the ratio of conductance increase due to the membrane flexibility does not change much for different temperatures (**Figure 2i**).

To understand the physical mechanism governing increased ion conductance due to the membrane flexibility, we analyzed pore expansion in flexible 2D membranes. **Figure 3a** shows that the pore radius is marginally larger in the flexible membranes than in the rigid membranes for Cu-HAB and GNM-3. The difference in pore radii of the rigid and flexible membranes for Cu-HAB and GNM-3 is 3.8% and 2.9%, respectively. The larger pore radii difference in Cu-HAB compared to that in GNM-3 is due to the lower mechanical stiffness in Cu-HAB ($34.0\ \mathrm{N/m}$) compared to that in GNM-3 ($61.2\ \mathrm{N/m}$)[21]. Ionic conductance theory can be used to analyze the contribution of pore expansion to ion conductance. Electrophoretic ion current is given by $I = \kappa\left(\frac{L}{\pi R^2} + \frac{1}{2R}\right)^{-1}\Delta\phi$ [26,50–52], where κ is the ionic conductivity, R is the nanopore radius, and $\Delta\phi$ is the electric potential difference. Using this theory, the nanopore enlargement in flexible membranes can only cause a small increase (up to 4%) in ionic conductance.

Membrane fluctuation, arising from membrane flexibility, is another important mechanism that has been shown to increase water transport at a certain frequency[21]. To understand the effect of membrane fluctuation on the ion conduction, we analyzed the trajectories of ions near the membranes. **Figures 3b and c** show the trajectories of potassium ions near the membranes with respect to time. The potassium ions diffuse more actively in the vicinity of the flexible Cu-HAB membrane compared to the rigid Cu-HAB membrane. For quantitative comparison, ion mobility

is calculated using the Einstein-Smoluchowski equation, $\mu = \frac{qD}{k_B T}$, where D is the diffusion coefficient, q is the charge of a particle, k_B is the Boltzmann constant, and T is the temperature. Ion mobilities near the 2D flexible membranes (within 5.5 Å from the membrane) are shown in **Figure 3d**. Ion mobility near the flexible Cu-HAB is about 117 to 142% greater than near the rigid Cu-HAB. On the other hand, ion mobility increases by about 25 to 29% near flexible GNM-3 compared to its rigid counterpart. On the other hand, the average ion concentration near the flexible membranes decreases slightly compared to the rigid membrane (1% decrease in GNM3 and 4% decrease in Cu-HAB). These indicate that the high ion conductance near flexible membranes is due to the high ion mobility near flexible membranes. The high ion mobility near the flexible membrane conforms with the study by Lyu *et al.*[42], which states that ion conductivity is higher in a flexible multilayered covalent organic framework compared to that in the rigid counterpart. It is noted that the ion mobility near the rigid membranes was lower compared to bulk mobility ($7.6 \times 10^{-8} \mathrm{m^2 V^{-1} s^{-1}}$ for potassium ion). However, ion mobility near the flexible Cu-HAB is higher compared to bulk mobility. Several studies have reported ion mobility higher than its bulk value in nanoscale channels/pores. Duan and Majumdar reported that the ion mobility in a 2 nm deep hydrophilic nanochannel is about 250% higher than bulk mobility[53]. Ma *et al.*[54] reported that ion mobility in a 3nm nanopore can be higher or lower compared to bulk mobility, depending on the ion concentration. In addition, studies showing the enhanced diffusion dynamics of fluid molecules confined to wiggling surfaces[40] and the longitudinal phonon mode of carbon nanotubes[39] supports our observations of improved ion mobility in flexible nanoporous membranes.

To further understand the impact of membrane fluctuations on ion mobility, we analyzed the velocity autocorrelation function (VACF) of ions near the membrane region. **Figures 3e-f**

show the VACF of ions near the membrane region. For Cu-HAB and GNM-3 membranes, ions experience forward scattering (*i.e.,* positive value of VACF) for the first few hundred femtoseconds, followed by backscattering (*i.e.,* negative value of VACF) for the remainder of time. **Figure 3e** shows that the fluctuations of Cu-HAB enhances the forward scattering and reduces backscattering. As a result, the ion mobility is increased. The ion mobility is calculated by the time integration of VACF: $\mu = \frac{q}{k_B T}\int_0^\infty \langle v(t\ +\ t_0)v(t_0)\rangle\, dt$, where v is the velocity of a particle, t_0 is the reference time, and the angle brackets denotes the time and ensemble average. On the other hand, the VACFs for ions near the GNM-3 membranes (**Figure 3f)** show that forward scattering is almost the same, and backscattering is slightly reduced in the flexible GNM-3 membrane compared to that in the rigid GNM-3 membrane. This analysis of VACFs indicates that the high ion conduction in fluctuating membranes is due to the dynamic coupling between the fluctuating membranes and nearby ions. This membrane-ion coupling is a surface phenomenon, and this mechanism leads to higher enhancements at low ion concentration where the surface conductance is dominant[26,55]. The impact of ion concentration on the enhanced ion conduction in flexible 2D membranes will be further investigated in a future study.

To understand the membrane-dependent increase in conductance, we analyzed how the frequency spectrum associated with membrane fluctuations affects nearby ion mobility. For this, additional MD simulations were run using oscillating membranes at various frequencies ω_s (**Figure 4a)**. In this conceptual study, the membrane oscillates in the out-of-plane direction following a simple sine function, and its average vibrational energy is assumed to be equal to the thermal energy. The VACFs of ions near the oscillating membranes are calculated (**Figure 4b)**. The oscillation of membrane enhances the forward scattering and reduces the backscattering, similar to what is observed in the flexible Cu-HAB. The degree of that effect (forward scattering

enchancement and backscattering reduction) depends on the membrane frequency and is maximized at the membrane frequency of around $200\ \mathrm{cm}^{-1}$. In addition, the ion conductance is considerably improved when the membrane oscillates with frequencies of $200\ \mathrm{cm}^{-1}$ (~135% increase compared to rigid counterpart). The conductance improvement is almost diminished in frequencies higher than $800\ \mathrm{cm}^{-1}$. We compared the range of frequency where the ion conduction is improved by computing the vibrational density of states (VDOS) for Cu-HAB and GNM-3. The VDOS is given by $\mathrm{VDOS}(\omega) = \int_{-\infty}^{\infty} \langle v(t+t_0)v(t_0)\rangle e^{-2\pi i\omega t} dt$. The VDOS for Cu-HAB and GNM-3 (**Figure 4d)** show that the Cu-HAB membrane exhibits high vibrational density in frequencies lower than $800\ \mathrm{cm}^{-1}$, where the ion conductance is improved. The GNM-3 membrane exhibits lower vibrational density compared to that exhibited by Cu-HAB in that frequency regime where ion conductance is improved. This explains the membrane-dependent conductance increase between the Cu-HAB and GNM-3 membranes.

We have identified two distinct frequency regimes in the resonance of a clamped membrane. The wiggling motions of the membrane, with frequencies significantly lower (approximately $0.05\ \mathrm{cm}^{-1}$ for a membrane with $L_{\mathrm{m}} = 4.62$ nm) than those of hydrated ions, are influenced by membrane size, shape, and tension. However, due to their low frequencies, these motions do not create significant vibrational coupling with nearby hydrated ions. Conversely, the atomic oscillations of the membrane, with frequencies ranging between $5\ \mathrm{cm}^{-1} \sim 1000\ \mathrm{cm}^{-1}$, exhibit strong vibrational coupling and are not influenced by the membrane's size.

To further understand the physical origin of the frequency range where conductance is high, we studied the vibrational frequency of hydrated ions. Ion dehydration[28,30] is one of the important mechanisms governing ion transport in Angstrom-scale. The ion-water stretching mode (**Figure 4e**) is the vibrational mode that is related to the ion dehydration. The VDOS of the

ion−water stretching modes (see the bottom plot of **Figure 4d**) exhibit a maximum at the frequency of around $200{\sim}300\ \mathrm{cm}^{-1}$, where the ion conductance is maximum. Moreover, we found that the vibrational match between a membrane and the ion−water stretching mode destabilizes the hydration shell of ions, enhancing ion conduction. The average hydration time τ_{hyd} is calculated by integrating the residence time autocorrelation function of water in the first hydration shell. **Figure 4f** displays the average hydration time for ions near membranes with different vibrational characteristics. The longest average hydration time is observed near the rigid Cu-HAB, where the atomic fluctuations are suppressed. This implies that ions near the rigid membrane form a relatively stable hydration shell that can hinder ion transport through Angstrom-scale pores. The hydration time is low near fluctuating membranes, and the average hydration time decreases as the membrane frequency approaches $200{\sim}300\ \mathrm{cm}^{-1}$. This suggests that the ion conduction and ion mobility near the membrane surface are improved due to the destabilized ion hydration when the frequency of the membrane fluctuation matches the ion–water stretching mode. This demonstrates that the type of electrolyte may potentially influence the degree of vibrational coupling and the enhancement of conductance. In terms of the effect of temperature, an increase in the temperature of system can increase the frequency of both the membrane and the hydrated ions. However, such frequency changes can only marginally alter the degree of vibrational coupling. This study expands the knowledge of ion transport by showing that the microscopic fluctuation of a membrane is an important factor in ion conduction across nanoporous membranes.

CONCLUSION

We observed that ion conductance in a flexible Cu-HAB membrane is approximately 102% higher compared to its rigid counterpart, whereas it is 9% higher in the flexible GNM-3 membrane compared to its rigid counterpart. Both potassium and chloride ions experience faster transport across flexible membranes. The increase in conductance exists irrespective of variations in ion concentration, ion type, and temperature. We observed a marginal pore expansion in flexible membranes, which slight increase in ionic conductance. Ion mobility is about 117% to 142% higher near flexible Cu-HAB and about 25% to 29% higher near flexible GNM-3 than their respective rigid counterparts. We found that the vibrational coupling between the fluctuating membrane and the ion−water stretching mode ($200\sim300\ \mathrm{cm}^{-1}$) destabilizes the ion hydration, which explains the membrane-dependent conductance enhancement between Cu-HAB and GNM-3. Our findings highlight the importance of microscopic fluctuations of 2D membranes in ion conduction. In addition, this phenomenon holds potential for manipulation of ion conduction by engineering the fluctuations of the membrane, which can be applied to various applications such as water purification, molecular separation, and electricity generation.

METHODS

We ran comprehensive MD simulations for ion transport across nanoporous membranes. As depicted in **Figure 1a**, the membrane is immersed in a 1.0 M KCl aqueous solution (we also tested different types of ions and different concentrations for some cases). The edges of a membrane are fixed, and the rest of the membrane is allowed to fluctuate during simulations. For comparison, we also considered cases with rigid membranes, where all the atoms of the membranes are fixed. To generate the electric potential gradient, we applied a uniform external electric field perpendicular to the membrane[56]. For all systems, the dimension perpendicular to the membrane is 5.80 nm. Periodic boundary conditions were applied in all directions. We considered two types of 2D membranes: Cu-HAB and GNM-3 (**Figures 1b and c**).[21] The size of the Cu-HAB membrane is 4.62 nm by 4.00 nm, and the size of the GNM-3 membrane is 5.01 nm by 4.43 nm. Both membranes contain 12 pores in a periodic cell. The electrolyte was modeled using the Coulombic and LJ potentials, and the membranes were modeled using the ReaxFF force field[57]. In the case of an oscillating membrane, the entire Cu-HAB membrane oscillates in the direction perpendicular to the membrane following $A \sin 2\pi\omega_s t$, where A is the amplitude, ω_s is the frequency, and t is the time. The vibrational energy was assumed to be equal to the thermal energy $\frac{Nk_BT}{2}$, where N is the number of atoms, k_B is the Boltzmann constant, and T is the temperature. The flexible simple point charge water model[58] was used for water. The potential parameters described by Joung *et al.*[59] were used for ions. ReaxFF potential parameters were adopted from Wood *et al.*[60] for GNM-3 and from Monti *et al.*[61] for Cu-HAB. The membrane-liquid interactions were modeled based on LJ and Coulombic potentials, and the LJ parameters are obtained from the Lorentz−Berthelot mixing rule (LJ parameters from Siu *et al.*[62] for hydrogen, Jorgensen *et al.*[63] for nitrogen, and Heinz *et al.*[64] for copper). The cut-off distance of the LJ potential was 1.2 nm. At the initial stage

of the MD simulation, the energy of the system was minimized. The partial charges of the membrane were calculated using the charge equilibration (QEq) method[65] and fixed during the simulation. The long-range Coulombic interactions were calculated using the particle-particle particle-mesh method[66] with an accuracy of 10^{-5}. The temperature of the system was maintained using the Nosé−Hoover thermostat at around the target temperature (298 K for most cases and 358 K for a few cases). Furthermore, atomic trajectories were computed in an NVT ensemble with 0.5 fs time interval[67]. The system was equilibrated for 1 ns and the data were obtained for 4 ns to calculate ion current. Ion current was calculated by counting the number of ions passing through the pores per unit time, and the mean squared displacement of ions was used to calculate the diffusion coefficient. We utilized the Large-scale Atomic/Molecular Massively Parallel Simulator (LAMMPS)[68] for MD simulations and the open visualization tool (OVITO)[69] for atomic visualizations.

ACKNOWLEDGMENTS

The work on graphene nanomembranes was supported by the Center for Enhanced Nanofluidic Transport (CENT), an Energy Frontier Research Center funded by the U.S. Department of Energy, Office of Science, Basic Energy Sciences (Award # DE-SC0019112). All other aspects of this work were supported by the National Science Foundation (NSF) under Grants 2140225 and 2137157. The computing power is provided by the Extreme Science and Engineering Discovery Environment (XSEDE) granted by NSF Grant No. OCI1053575 and Blue Waters supercomputing center, awarded by the state of Illinois and NSF, OCI-0725070, ACI-1238993.

AUTHOR CONTRIBUTIONS

Y.N performed simulations, analysis, and wrote the manuscript under the guidance of N.A.

DECLARATION OF INTERESTS

The authors declare no competing interests.

REFERENCES

1 K. Kunzelmann, *J Membrane Biol*, 2005, **205**, 159–173.

2 A. L. Gotter, M. A. Kaetzel and J. R. Dedman, *Comparative Biochemistry and Physiology Part A: Molecular & Integrative Physiology*, 1998, **119**, 225–241.

3 K. Xiao, L. Jiang and M. Antonietti, *Joule*, 2019, **3**, 2364–2380.

4 M. A. El-Sayed, *Acc. Chem. Res.*, 1992, **25**, 279–286.

5 S. Y. Noskov, S. Bernèche and B. Roux, *Nature*, 2004, **431**, 830–834.

6 C. Duran, C. H. Thompson, Q. Xiao and H. C. Hartzell, *Annual Review of Physiology*, 2010, **72**, 95–121.

7 R. B. Stockbridge, L. Kolmakova-Partensky, T. Shane, A. Koide, S. Koide, C. Miller and S. Newstead, *Nature*, 2015, **525**, 548–551.

8 S. Bernèche and B. Roux, *Nature*, 2001, **414**, 73–77.

9 M. Zhou, J. H. Morais-Cabral, S. Mann and R. MacKinnon, *Nature*, 2001, **411**, 657–661.

10 S.-L. Cai, Y.-B. Zheng, S.-H. Cao, X.-H. Cai and Y.-Q. Li, *Chemical Communications*, 2016, **52**, 12450–12453.

11 D. Basu and E. S. Haswell, *Current Opinion in Plant Biology*, 2017, **40**, 43–48.

12 A. Anishkin, S. H. Loukin, J. Teng and C. Kung, *PNAS*, 2014, **111**, 7898–7905.

13 Y. Feng, W. Zhu, W. Guo and L. Jiang, *Advanced Materials*, 2017, **29**, 1702773.

14 J. Feng, M. Graf, K. Liu, D. Ovchinnikov, D. Dumcenco, M. Heiranian, V. Nandigana, N. R. Aluru, A. Kis and A. Radenovic, *Nature*, 2016, **536**, 197.

15 X. Li, H. Zhang, P. Wang, J. Hou, J. Lu, C. D. Easton, X. Zhang, M. R. Hill, A. W. Thornton, J. Z. Liu, B. D. Freeman, A. J. Hill, L. Jiang and H. Wang, *Nat Commun*, 2019, **10**, 2490.

16 H. Qi, Z. Li, Y. Tao, W. Zhao, K. Lin, Z. Ni, C. Jin, Y. Zhang, K. Bi and Y. Chen, *Nanoscale*, 2018, **10**, 5350–5357.

17 S. J. Heerema and C. Dekker, *Nature Nanotech*, 2016, **11**, 127–136.

18 K. Liu, J. Feng, A. Kis and A. Radenovic, *ACS nano*, 2014, **8**, 2504.

19 Z. Cao, V. Liu and A. Barati Farimani, *Nano Lett.*, 2019, **19**, 8638–8643.

20 D. Cohen-Tanugi and J. C. Grossman, *Nano Lett.*, 2012, **12**, 3602–3608.

21 Y. Noh and N. R. Aluru, *Nano Lett.*, 2022, **22**, 419–425.

22 Y. Yang, X. Yang, L. Liang, Y. Gao, H. Cheng, X. Li, M. Zou, R. Ma, Q. Yuan and X. Duan, *Science*, 2019, **364**, 1057–1062.

23 C. Moreno, M. Vilas-Varela, B. Kretz, A. Garcia-Lekue, M. V. Costache, M. Paradinas, M. Panighel, G. Ceballos, S. O. Valenzuela, D. Peña and A. Mugarza, *Science*, 2018, **360**, 199–203.

24 Y. Zhong, B. Cheng, C. Park, A. Ray, S. Brown, F. Mujid, J.-U. Lee, H. Zhou, J. Suh, K.-H. Lee, A. J. Mannix, K. Kang, S. J. Sibener, D. A. Muller and J. Park, *Science*, 2019, **366**, 1379–1384.

25 D. Feng, T. Lei, M. R. Lukatskaya, J. Park, Z. Huang, M. Lee, L. Shaw, S. Chen, A. A. Yakovenko, A. Kulkarni, J. Xiao, K. Fredrickson, J. B. Tok, X. Zou, Y. Cui and Z. Bao, *Nature Energy*, 2018, **3**, 30–36.

26 Y. Noh and N. R. Aluru, *ACS Nano*, 2020, **14**, 10518–10526.

27 Myung E. Suk and N. R. Aluru, Ion transport in sub-5-nm graphene nanopores: The Journal of Chemical Physics: Vol 140, No 8, https://aip.scitation.org/doi/abs/10.1063/1.4866643, (accessed March 19, 2019).

28 S. Sahu, M. Di Ventra and M. Zwolak, *Nano Lett.*, 2017, **17**, 4719–4724.

29 Z. Li, Y. Qiu, Y. Zhang, M. Yue and Y. Chen, *J. Phys. Chem. C*, 2019, **123**, 15314–15322.

30 Z. He, J. Zhou, X. Lu and B. Corry, *ACS Nano*, 2013, **7**, 10148–10157.

31 A. Fang, K. Kroenlein, D. Riccardi and A. Smolyanitsky, *Nature Mater*, 2019, **18**, 76–81.

32 A. Smolyanitsky, A. Fang, A. F. Kazakov and E. Paulechka, *Nanoscale*, 2020, **12**, 10328–10334.

33 A. Gadaleta, C. Sempere, S. Gravelle, A. Siria, R. Fulcrand, C. Ybert and L. Bocquet, *Physics of Fluids*, 2014, **26**, 012005.

34 K. Yazda, K. Bleau, Y. Zhang, X. Capaldi, T. St-Denis, P. Grutter and W. W. Reisner, *Nano Lett.*, 2021, **21**, 4152–4159.

35 M. Tsutsui, K. Yokota, I. W. Leong, Y. He and T. Kawai, *Cell Reports Physical Science*, 2022, **3**, 101065.

36 K. Sint, B. Wang and P. Král, *J. Am. Chem. Soc.*, 2008, **130**, 16448–16449.

37 X. Jiang, C. Zhao, Y. Noh, Y. Xu, Y. Chen, F. Chen, L. Ma, W. Ren, N. R. Aluru and J. Feng, *Science Advances*, 2022, **8**, eabj2510.

38 A. Kohen, R. Cannio, S. Bartolucci, J. P. Klinman and J. P. Klinman, *Nature*, 1999, **399**, 496–499.

39 M. Ma, F. Grey, L. Shen, M. Urbakh, S. Wu, J. Z. Liu, Y. Liu and Q. Zheng, *Nature Nanotechnology*, 2015, **10**, 692–695.

40 S. Marbach, D. S. Dean and L. Bocquet, *Nature Physics*, 2018, **14**, 1108–1113.

41 Y. Noh and N. R. Aluru, *Phys. Rev. E*, 2022, **106**, 025106.

42 B. Lyu, M. Wang, Z. Jiang and J. Jiang, *Journal of Membrane Science*, 2022, **658**, 120754.

43 N. Lahiri, N. Lotfizadeh, R. Tsuchikawa, V. V. Deshpande and J. Louie, *J. Am. Chem. Soc.*, 2017, **139**, 19–22.

44 J. Bai, X. Zhong, S. Jiang, Y. Huang and X. Duan, *Nature Nanotech*, 2010, **5**, 190–194.

45 G. Tronci, F. Raffone and G. Cicero, *Applied Sciences*, 2018, **8**, 1547.

46 S. Zhao, J. Xue and W. Kang, *J. Chem. Phys.*, 2013, **139**, 114702.

47 L. E. Kreno, K. Leong, O. K. Farha, M. Allendorf, R. P. Van Duyne and J. T. Hupp, *Chem. Rev.*, 2012, **112**, 1105–1125.

48 J. Lee, O. K. Farha, J. Roberts, K. A. Scheidt, S. T. Nguyen and J. T. Hupp, *Chemical Society Reviews*, 2009, **38**, 1450–1459.

49 H. Wang, Q.-L. Zhu, R. Zou and Q. Xu, *Chem*, 2017, **2**, 52–80.

50 S. Rm, K. Uf, K. D, W. My, D. Nh and D. C, *Nano Lett*, 2006, **6**, 89–95.

51 A. Kumar, K.-B. Park, H.-M. Kim and K.-B. Kim, *Nanotechnology*, 2013, **24**, 495503.

52 S. W. Kowalczyk, A. Y. Grosberg, Y. Rabin and C. Dekker, *Nanotechnology*, 2011, **22**, 315101.

53 C. Duan and A. Majumdar, *Nature Nanotech*, 2010, **5**, 848–852.

54 J. Ma, K. Li, Z. Li, Y. Qiu, W. Si, Y. Ge, J. Sha, L. Liu, X. Xie, H. Yi, Z. Ni, D. Li and Y. Chen, *J. Am. Chem. Soc.*, 2019, **141**, 4264–4272.

55 D. Stein, M. Kruithof and C. Dekker, *Phys. Rev. Lett.*, 2004, **93**, 035901.

56 J. Gumbart, F. Khalili-Araghi, M. Sotomayor and B. Roux, *Biochimica et Biophysica Acta (BBA) - Biomembranes*, 2012, **1818**, 294–302.

57 A. C. T. van Duin, S. Dasgupta, F. Lorant and W. A. Goddard, *J. Phys. Chem. A*, 2001, **105**, 9396–9409.

58 Y. Wu, H. L. Tepper and G. A. Voth, *J. Chem. Phys.*, 2006, **124**, 024503.

59 I. S. Joung and T. E. Cheatham, *The Journal of Physical Chemistry. B*, , DOI:10.1021/jp8001614.

60 M. A. Wood, A. C. T. van Duin and A. Strachan, *J. Phys. Chem. A*, 2014, **118**, 885–895.

61 S. Monti, C. Li and V. Carravetta, *J. Phys. Chem. C*, 2013, **117**, 5221–5228.

62 S. W. I. Siu, K. Pluhackova and R. A. Böckmann, *J. Chem. Theory Comput.*, 2012, **8**, 1459–1470.

63 W. L. Jorgensen, D. S. Maxwell and J. Tirado-Rives, *J. Am. Chem. Soc.*, 1996, **118**, 11225–11236.

64 H. Heinz, R. A. Vaia, B. L. Farmer and R. R. Naik, *The Journal of Physical Chemistry C*, 2008, **112**, 17281–17290.

65 A. K. Rappe and W. A. Goddard, *J. Phys. Chem.*, 1991, **95**, 3358–3363.

66 R. W. Hockney and J. W. Eastwood, *Computer Simulation Using Particles, New York: McGraw-Hill, 1981*.

67 B. D. Jensen, K. E. Wise and G. M. Odegard, *Journal of Computational Chemistry*, 2015, **36**, 1587–1596.

68 S. Plimpton, *Journal of Computational Physics*, 1995, **117**, 1–19.

69 A. Stukowski, *Modelling and Simulation in Materials Science and Engineering*, 2010, **18**, 015012.

LIST OF FIGURES

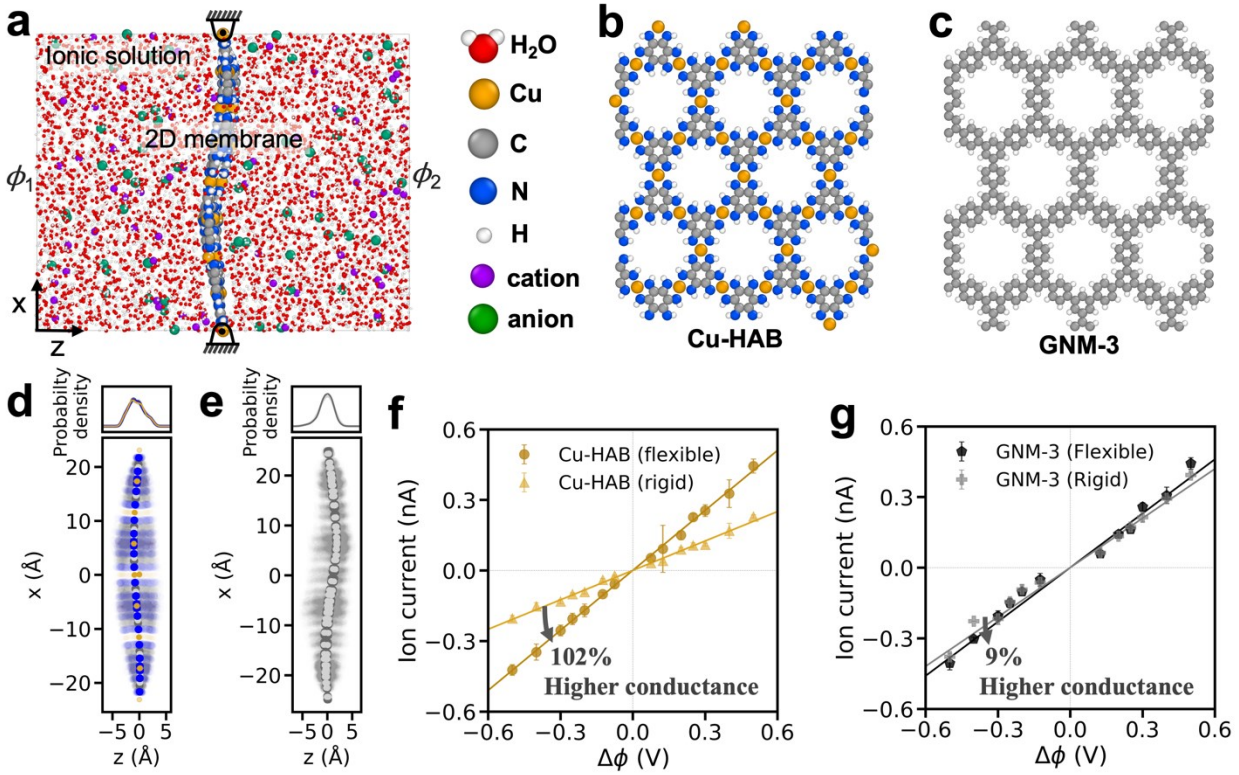

Figure 1 | Ion transport across 2D flexible nanoporous membranes. a. MD simulation setup for ion transport. The 2D membrane is immersed in an electrolyte solution, and its edges are constrained. A cross-membrane electric potential difference is applied. Atomic structure of **b.** Cu-HAB and **c.** GNM-3. Fluctuations of **d.** Cu-HAB and **e.** GNM-3 (bottom) and its distribution (top). The opaque colors indicate the mean position of the membrane. The transparent colors indicate the membrane fluctuations. Current–voltage characteristics in **f.** Cu-HAB and **g.** GNM-3 membranes. The plotted ion currents are divided by the number of nanopores (*i.e.,* 12) in the membrane. The solid lines represent a linear fit to the MD data.

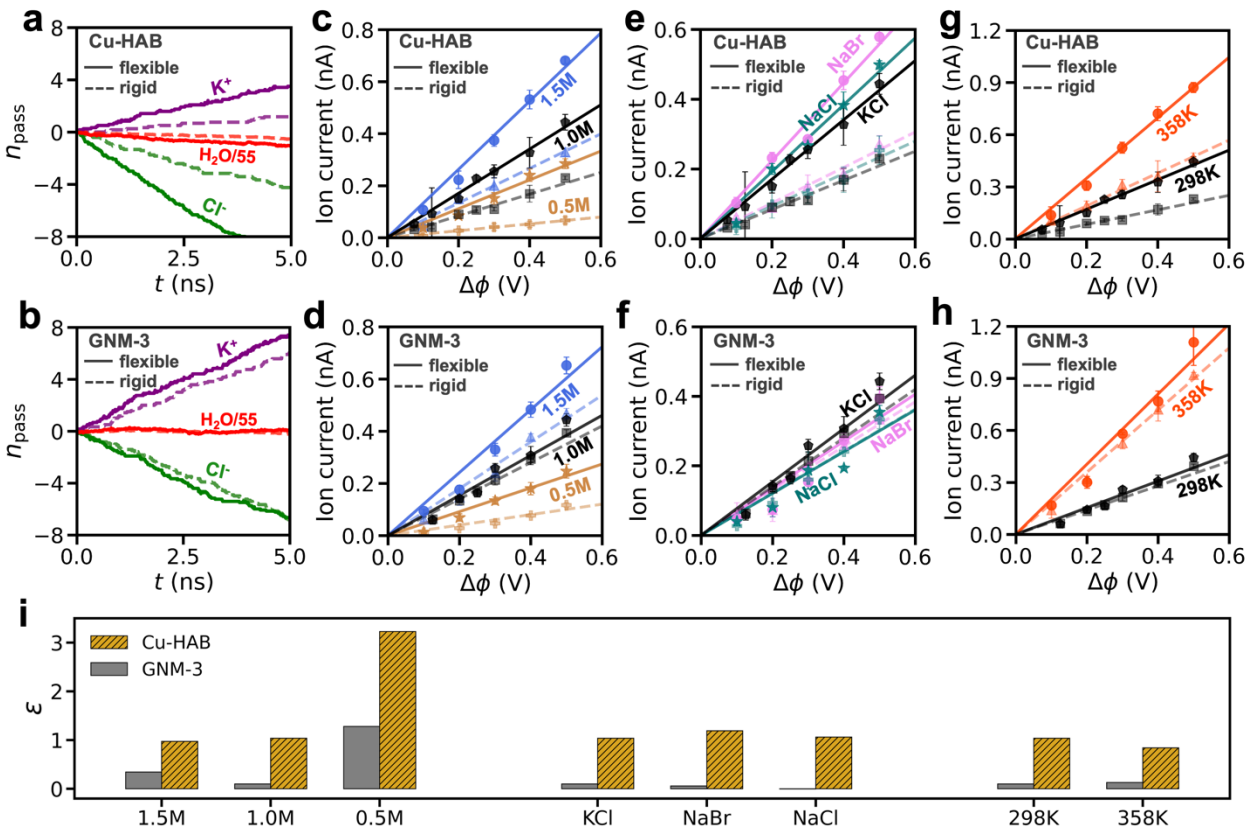

Figure 2 | Ion transport for various parameters. The number of molecules transported across the membranes per pore, n_{pass}, over time in **a.** Cu-HAB and **b.** GNM-3 at 0.5 V. In the plot, n_{pass} for water molecules are reduced by the factor of the ratio between the densities of water and ion (*i.e.,* 55 for 1.0 M solution). Current–voltage curves for different concentrations of KCl solution at 298 K in **c.** Cu-HAB and **d.** GNM-3. Current–voltage curves for different types of ions for 1.0 M concentration at 298 K in **e.** Cu-HAB and **f.** GNM-3. Current–voltage curves for different temperatures for 1.0 M KCl solution in **g.** Cu-HAB and **h.** GNM-3. The symbols with solid and transparent colors represent flexible and rigid membranes, respectively. The solid and dashed lines represent a linear fit to the MD data. **i.** The increase in ion conductance in flexible membrane over its rigid counterpart is given by $\varepsilon = \left(G_{\text{flexible}} - G_{\text{Rigid}}\right)/G_{\text{Rigid}}$**.** The effect of different parameters (concentration, type of ion and temperature) is shown.

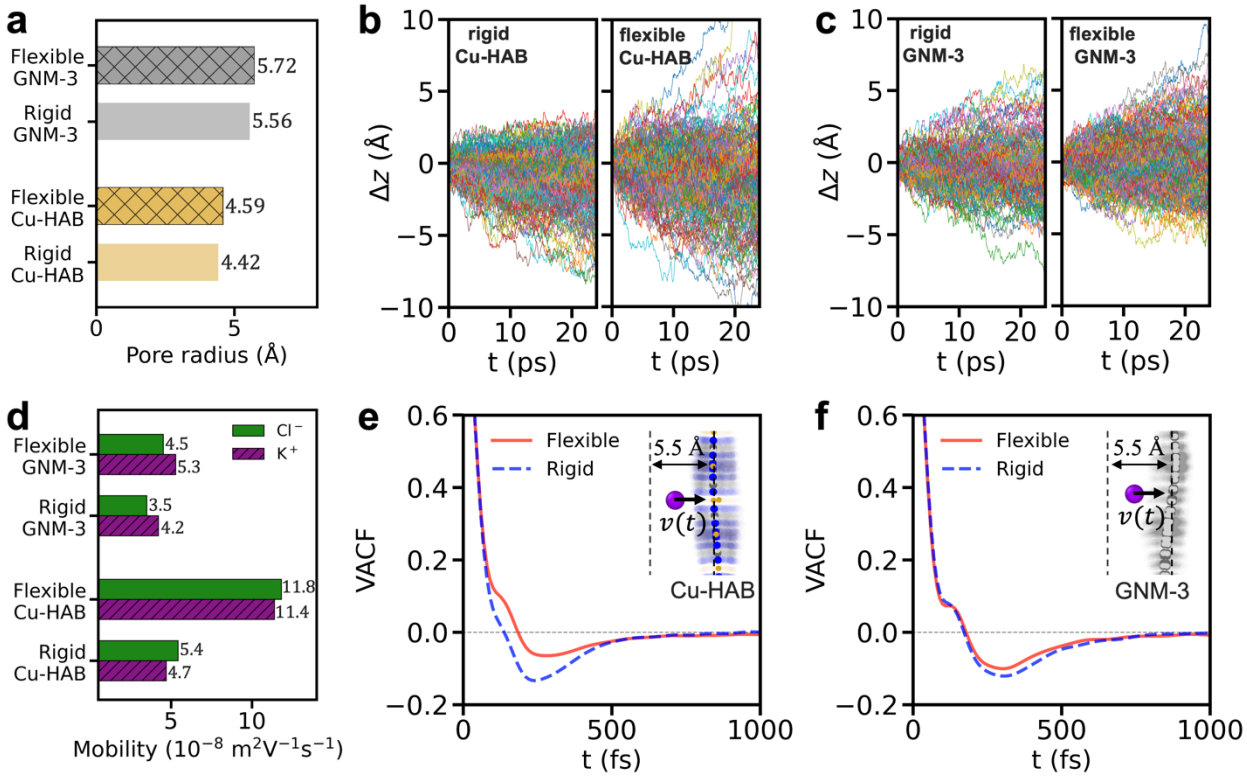

Figure 3 | Pore expansion and increase in ion mobility in flexible membranes. a. Pore radius. Trajectories of potassium ions near **b.** rigid Cu-HAB (left), flexible Cu-HAB (right), **c.** rigid GNM-3 (left), and flexible GNM-3 (right). The displacement is given by $\Delta z(t) = z(t) - z(t_0)$ for $-5.5\ \text{Å} \leq z(t_0) \leq 0$, where t_0 is the reference time. **d.** Mobility of ions near the membranes. Velocity autocorrelation function (VACF) of potassium ions near **e.** Cu-HAB and **f.** GNM-3. VACF is given by $\langle v(t + t_0)v(t_0)\rangle / \langle v(t_0)v(t_0)\rangle$ for $-5.5\ \text{Å} \leq z(t_0) \leq 0$. The insets show the "near the membranes" region used in this study.

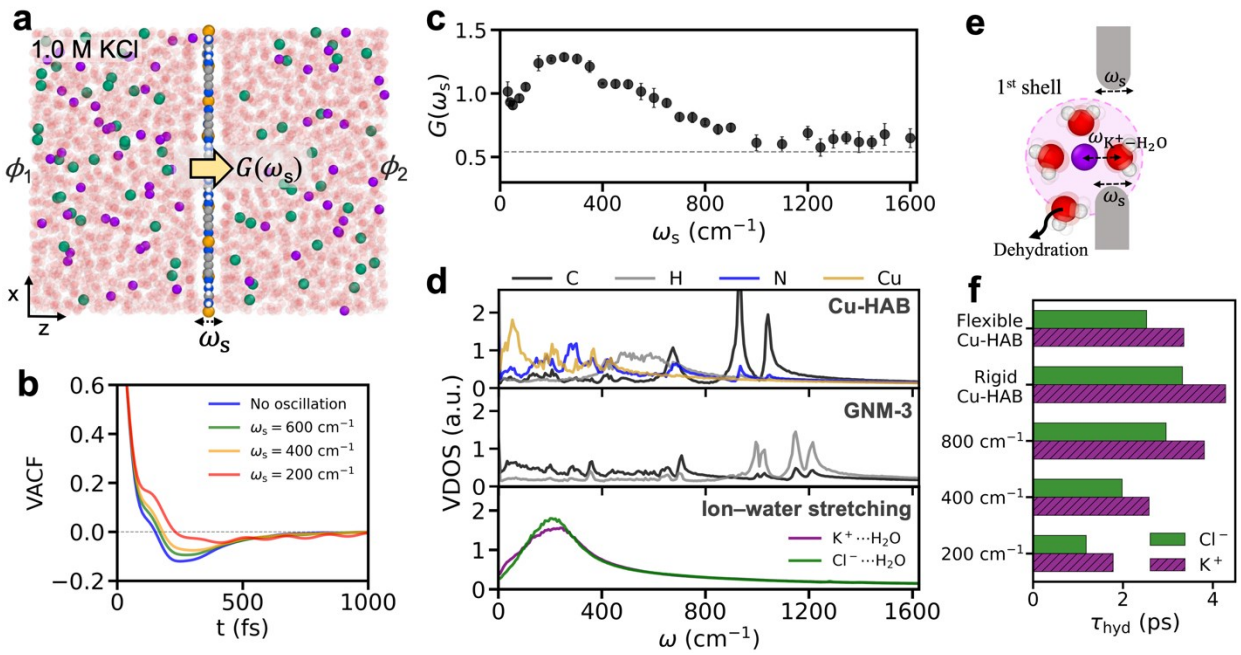

Figure 4 | Ion transport through oscillating membranes. a. System for MD simulation. The entire membrane oscillates harmonically with a frequency ω_s in the out-of-plane direction. **b.** The VACF for potassium ions near the membrane for various ω_s. **c.** Ion conductance for various ω_s. The gray dashed line represents the conductance in rigid Cu-HAB. **d.** Vibrational density of states for the flexible Cu-HAB**,** the flexible GNM-3, and ion–water stretching mode (membrane fluctuation data are obtained from the system described in **Figure 1a**). **e**. Schematic of dehydration near the oscillating membrane. **f.** average hydration time near membranes for different vibrational characteristics.

GRAPHISCAL ABSTRACT